

Modeling the Effect of Residual and Diffusion-Induced Stresses on Corrosion at the Interface of Coating and Substrate

M.H. Nazir,^{†,*} Z.A. Khan,^{*} A. Saeed,^{*} and K. Stokes^{**}

ABSTRACT

The effect of residual and diffusion-induced stresses on corrosion at the interface of coating and substrate has been analyzed within a multidisciplinary approach, i.e., material science, solid mechanics, and electrochemistry. A self-consistent equation for corrosion current density, involving the combined effect of residual stress and diffusion-induced stress is developed. The influences of temperature, moduli ratio, thickness ratio, thermal mismatch ratio, and residual stress gradient of coating and substrate on the corrosion current density are then discussed. Results indicate that when the thermal expansion of coating is greater than substrate, the decrease in temperature from fabrication temperature accounts for the same direction of both the residual and the diffusion stresses. This behavior increases the deflection of the coating-substrate system and results in the evolution of tensile residual stress in the coating. The tensile stress opens the pre-existing coating microcrack, allowing the diffusion of corrosive agents and therefore, accelerating the corrosion damage to the coating/substrate interface. The model is based on experimental observations conducted to understand the behavior of corrosion at the coating/substrate interface in the presence of tensile or compressive residual stresses. At the end, the model was validated against the experimental results showing a good quantitative agreement between the predicted theoretical and experimental trends.

KEY WORDS: blister, coating, coating failure, corrosion, delamination, diffusion-induced stress, iterative algorithm, mathematical modeling, partial differential equations, residual stress

INTRODUCTION

Recent studies have shown that the corrosion of steel-based infrastructures is estimated to cost about 3% of global gross domestic product (GDP) each year.¹ To combat and control the corrosion of metals, various methods are deployed to mitigate the high direct and indirect costs of corrosion.²⁻⁴ The most common method of prevention against corrosion uses organic coatings.⁵⁻⁶ The organic coatings are used to isolate the metal from its surrounding environment by using a physical barrier.

Based on experimentation performed in this paper, it was concluded that the failure of coating-substrate system depends on three interdependent causes. (i) Corrosion current density “*i*”: a corrosion sensor adhered to the substrate, beneath the coating, measures the corrosion current density. (ii) Tensile/compressive residual stress: the corrosion current density directly depends upon the development of tensile or compressive residual stresses on the coating. These stresses develop, as a result of mismatches in coefficients of thermal expansion (CTE), when subjected to the change in temperature, ΔT , from fabrication temperature. (iii) Electrolyte diffusion: temperature change directly controls the electrolyte diffusion toward the interface, subject to CTE mismatch. All of these three causes are interdependent but fall under “three”

Submitted for publication: June 7, 2015. Revised and accepted: December 9, 2015. Preprint available online: December 9, 2015, <http://dx.doi.org/10.5006/1804>.

[†] Corresponding author. E-mail: hnazir@bournemouth.ac.uk.

^{*} Bournemouth University, NanoCorr, Energy and Modeling (NCEM) Research Group, Faculty of Science and Technology, Bournemouth University, United Kingdom.

^{**} Defence Science and Technology Laboratory (DSTL), Ministry of Defence (MoD), Salisbury, United Kingdom.

different disciplines. Corrosion current density uses electrochemistry concepts, tensile/compressive residual stress uses solid mechanics concepts, and electrolyte diffusion uses material science concepts.

Although corrosion is an electrochemical reaction, the process is strongly influenced by the mechanical and microstructural properties of materials.⁷ In addition, the corrosion resistance of a coated steel sample is also affected by microcracks in the coating.⁸ These microcracks may act as pathways for corrosive agents to diffuse through the coating barrier, which may result in the initiation of localized corrosion in the less noble metal substrate.⁹ Stress corrosion cracking (SCC), resulting from growth of crack formation in a corrosive environment, results when the metals are subjected to tensile residual stress in a corrosive environment.¹⁰⁻¹² Contrary to this, compressive residual stress results in the inhibition of the corrosion of metals.¹³⁻¹⁴ In addition to residual stress, the chemical stress (or diffusion-induced stress) also influences the SCC and, therefore, affects the stability and reliability of materials.¹⁵ The coupling effect of residual stress and diffusion-induced stress on the propagation of corrosion at the coating/substrate interface has not been investigated in detail in the existing literature. It is therefore essential to analyze the propagation of corrosion at the interface of coating and substrate in consideration of the coupling effects of residual and diffusion-induced stresses.

For the residual stress (strain) analysis, the Stoney formula has been extensively used in the literature to infer coating stress changes from experimental measurement of system curvature changes.¹⁶ Based on Stoney's formula, some of the modified models have been developed by Huang and Zhang,¹⁷ Soliman and Waheed,¹⁸ Clyne and Gill,¹⁹ Widjaja, et al.,²⁰ Zhang, et al.,²¹ Wisnom, et al.,²² and Bansal, et al.,²³ to address advance and better closed-form solutions of the uniformed residual strain in the coatings. Later on it was identified, with the help of finite element analysis, that the propagation of corrosion at the interface of coating and substrate is inhibited by compressive residual stress, which causes the contraction of open corrosion paths in the coatings.²⁴ However, the results from the model²⁴ showed only the limited effect of compressive residual stress on the cross-sectional area of corrosion pits. The model did not address the effects of the compressive residual stress over pre-existing structural microcracks in the coatings. These microcracks in the presence of compressive residual stress contract, and can inhibit the diffusion of corrosive agents through the coating and result in lower corrosion rate at the interface of coating and substrate.

Meanwhile, the diffusion-induced stress has drawn a considerable interest in the previous decades.²⁵⁻²⁶ For the diffusion-induced stress, various numerical models have been available since the

pioneering work of Podstrigach and Shevchuk.²⁷ Later on, some modified numerical models were developed by researchers²⁸⁻³² after a series of studies on diffusion-induced stress in the coating-substrate system. In recent research work, various numerical methods and advanced techniques for the coating-substrate delamination involving diffusion-induced stresses have been developed by Nguyen, et al.,³³ Prawoto, et al.,³⁴ Zhang, et al.,²¹ Yang and Li,³⁵ and Rusanov.³⁶ However, the occurrence of the residual stress in the coating-substrate system resulting from mismatch in thermal expansion cannot be neglected; therefore, both the diffusivity and concentration of corrosive agents will be enhanced by the hydrostatic stress. The existing stress may speed up or hinder the diffusivity depending upon the direction of stress gradient.

Previous research has modeled³⁷⁻⁴⁹ to address the coating-substrate failure in the individual disciplines. However, there is a missing link in modeling between the three distinct disciplines, which can combine the three disciplines to address majority of coating failure related issues. In order to address the missing link between these three disciplines, a mathematical model has been developed in the next sections. The newly developed mathematical model follows a multidisciplinary approach which fosters a close collaboration between three major disciplines, i.e., material science, solid mechanics, and electrochemistry. The purpose of this work is to analyze corrosion at the interface of coating and substrate, induced by diffusion in the presence of residual stress. The model involves the coupling effects of electrochemical reactions resulting from corrosion at the interface, with the residual stress and diffusion-induced stress in a coating-substrate system. Then, the solution of corrosion current density at the interface is derived involving the feedback of residual stress to the diffusion of corrosive agent through coating. The evolution of corrosion current density corresponding to different moduli ratio, thickness ratio, thermal expansion mismatch ratio, and residual stress gradients of coating and substrate have been discussed in terms of Newton-Raphson method. Finally, validation of the developed model is performed and a comparison is developed between simulated and experimental results.

EXPERIMENTAL PROCEDURES

Sample Preparation

A thin carbon steel panel with a thickness of $s = 1/20$ in (1 mm) was used to prepare three test samples with dimensions 6 in \times 4 in each. The coefficient of thermal expansion (CTE) and Young's modulus for the steel are $\alpha_s = 11.7 \times 10^{-6} \text{ K}^{-1}$ and $E_s = 200 \text{ GPa}$, respectively.⁵⁰ Prior to coating deposition, surface conditioning is deployed by using a polishing wheel with emery paper of 200 grit size. After polishing, the

conditioned samples were cleaned with a 35 min immersion into a constantly stirred solution of 50 g/L Turco 4215 NC-LT[†]. After completing this alkaline cleaning, the samples were rinsed with deionized water and air dried. Weight was recorded to the nearest fifth significant digit and the steel samples were stored in a desiccator. To ensure the repeatability, the experimental data was collected from three samples each adhered with corrosion sensor with dimensions of 40 mm × 20 mm × 0.1 mm. These sensors⁵¹ consisted of multiple plates made from the material of interest which formed the two electrodes. The electrodes were used in conjunction with a potentiostat for conducting linear polarization resistance (LPR) measurements. The use of a relatively large counter electrode minimized polarization effects at the counter electrode to ensure that a stable reference potential was maintained throughout the experiments. Potential step-sweeps were performed by applying a series of 30 steps over a range of ±10 mV spanning a period of 2.6 s.⁵²

Corrosion sensors measure the polarization resistance R_p (Ω) between the corrosive agents (electrolytic solution) and the steel samples. The polarization resistance is then used to calculate the corrosion current density “ i ” at the interface by using Stern-Geary equation as:⁵³

$$i = B/R_p \quad (1)$$

where B is the Stern-Geary constant. The corrosion current density is measured from the polarization resistance values by using a Stern-Geary constant of 30 mV for carbon steel.⁵²

The corrosion sensors were adhered to the conditioned face of the steel samples with industrial strength epoxy, as shown in Figure 1. The bonding agent (industrial strength epoxy) was placed on the opposite edges of the sensors so as to adhere the sensors to the conditioned surface of the steel samples in a manner such that the ambient environment is allowed to rapidly diffuse between the sensors and the steel. The sensor array included at least two interlaced inert electrodes that were manufactured from a noble metal. The noble metal options were Au, Pt, and Pd because of the low contact resistances. The noble metals were principally inert, such that the sensor array did not readily corrode in typical ambient environments.

After installation of corrosion sensors on steel samples, the samples were applied with the thin coating (primer red oxide) by using a conventional spray gun at the temperature of 318 K (45°C); this is shown in Figure 1. The thickness of the coating was $h = 0.020$ mm. The coefficient of thermal expansion CTE ($\alpha_c = 21.6 \times 10^{-6} \text{ K}^{-1}$) and Young's modulus ($E_c = 6.14 \text{ GPa}$) for the thin coating were measured by using thermomechanical analysis test according

[†] Trade name.

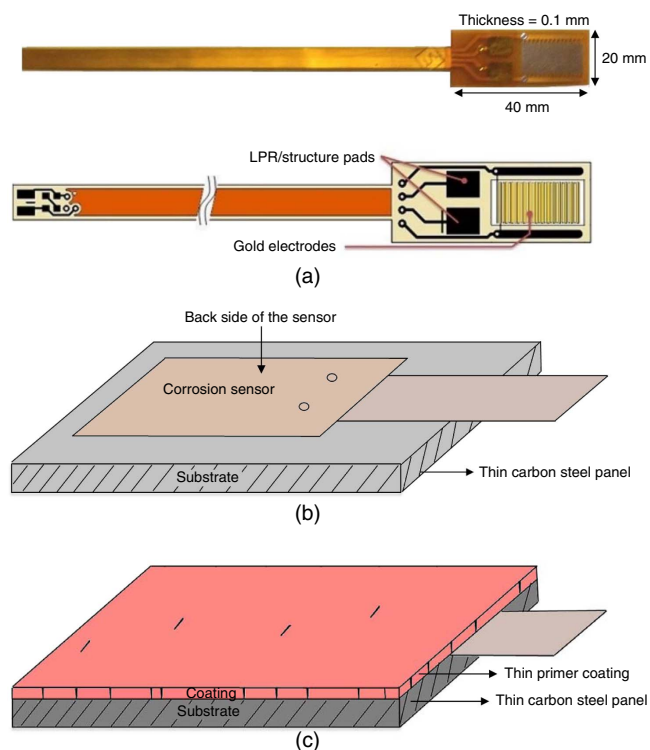


FIGURE 1. (a) The corrosion sensor.⁵² (b) Installation of corrosion sensor on steel sample, (c) applied with the thin coating (referred to as primer) by using a conventional spraying gun at temperature of 318 K (45°C).

to the procedures of ASTM E831-14⁵⁴ and ASTM E2769-13,⁵⁵ respectively. The coating was allowed to fully seal over a 24 h period at 318 K before testing. The temperature of 318 K is referred to as the fabrication temperature of the coating-substrate system.

Accelerated Corrosion Testing

Accelerated corrosion testing was performed in a corrosive atmosphere chamber. The electrolyte solution composing the fog was 5 parts of sodium chloride in 95 parts of deionized water. The samples were positioned at a 60° angle inside the chamber with the coated face downward, as to avoid the direct pathway for condensate into the coating. Electrical connections for the corrosion sensors were made to a data acquisition unit (DAU) positioned outside the chamber by passing extension cables through a bulkhead, as shown in Figure 2. Temperature and corrosion data were acquired at 1 min intervals.

Accelerated corrosion testing was conducted for a total time of 50 h and consisted of five steps each (10 h per step), as shown in Figure 3. The purpose of these steps was to analyze the corrosion current density at coating/substrate interface corresponding to various stress levels in coating at different temperatures. The first step involved exposing the samples to a salt fog for a period of 10 h at fabrication temperature,

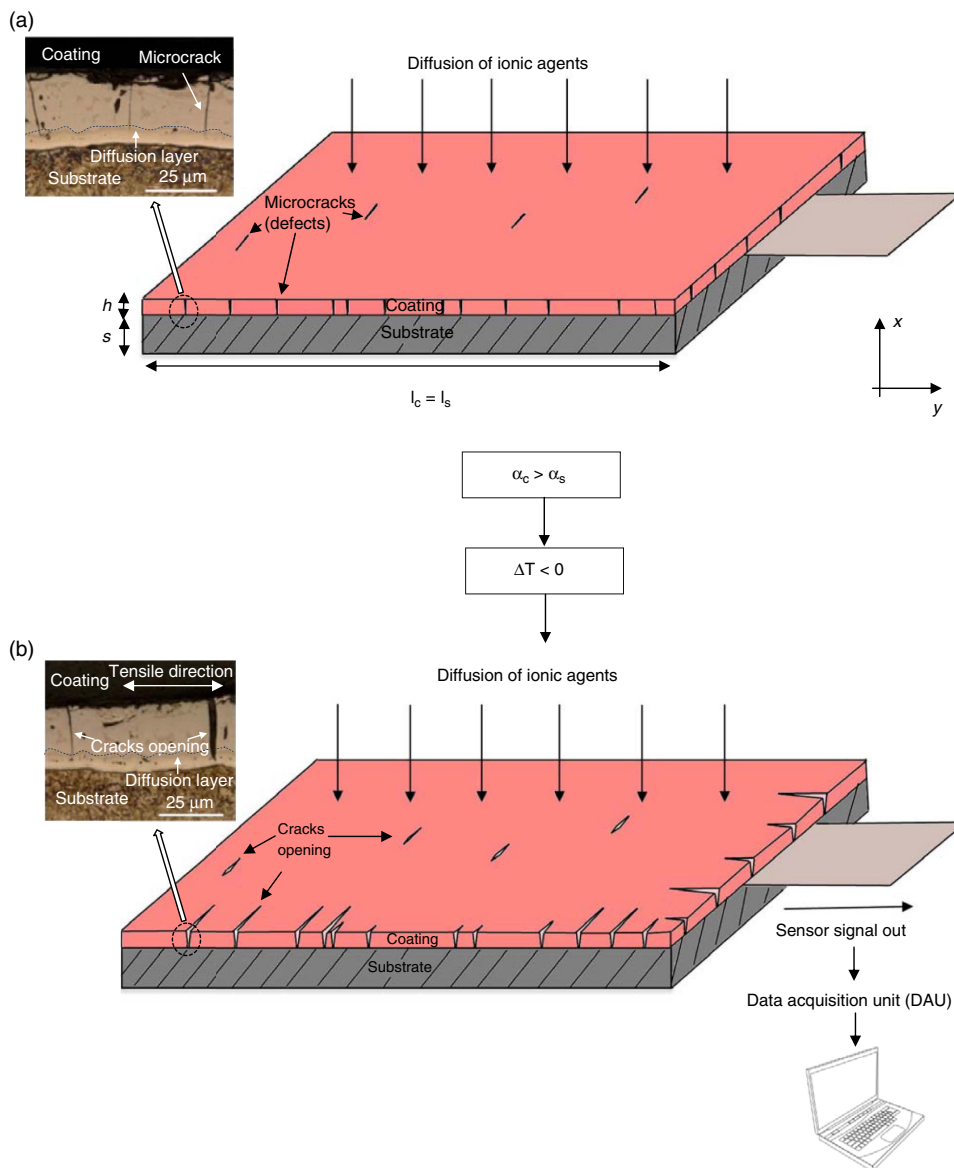


FIGURE 2. (a) Accelerated corrosion testing of primer coated steel sample in a corrosive atmosphere chamber. (b) Because the CTE of thin primer is greater than the steel substrate, i.e., $\alpha_c > \alpha_s$, negative temperature change ($\Delta T < 0$) accounts for the tensile residual stress in the coating. The tensile residual stress allows the opening of pre-existing coating defects resulting in the evolution of corrosion at the interface. The corrosion rate at the coating/substrate interface is monitored by a corrosion sensor connected to computer through DAU.

i.e., 318 K (45°C). For this period of time, ΔT is equal to 0 ± 1 K, as the final temperature (318 ± 1 K) and fabrication temperature of coating-substrate system (318 K) were almost same. ΔT is calculated by using Equation (1).

$$\Delta T = \text{Final Temperature} - \text{Fabrication Temperature} \quad (2)$$

The second step involved reducing the temperature from 318 K to 303 ± 2 K ($29.8 \pm 2^\circ\text{C}$) and maintaining this temperature for a period of 10 h, while keeping the same level of fog inside the chamber. The third step involved increasing the temperature from 303 ± 2 K to

318 K and maintaining this temperature for a period of 10 h. The fourth step involved again reducing the temperature from 318 K to 311 ± 3 K and maintaining for 10 h, followed by the last step in which the temperature was again increased and maintained at 318 K for last 10 h of the experiment.

Experimental Observations

The corrosion sensors adhered to the substrate beneath the coating determine the corrosion current density based upon electrolyte conductivity, ionic strength of electrolyte, and temperature. Corrosion at

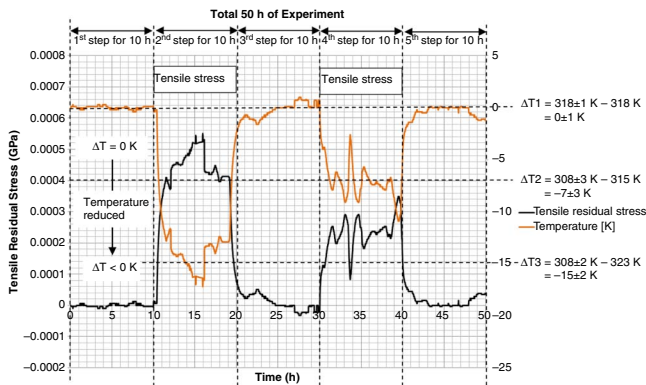


FIGURE 3. Graph showing the tensile residual stress, which is developed in the coating by reducing the temperature (in the second and fourth step of experimentation) inside the chamber.

the interface of the coating and substrate is primarily controlled by the concentration of an electrolyte solution and the temperature. The concentration is controlled by the residual stress in the coating, which is caused by temperature difference, ΔT . The residual stress can either block the pathway of corrosive agents (as a result of compressive behavior) by constricting the pre-existing coating microcracks or open the pathway of corrosive agents (as a result of tensile behavior) by exposing the pre-existing coating microcracks.

The elastic response of coating suffered from the residual stress and diffusion-induced stress is analyzed in terms of the principle of linear superposition.⁵⁶ Because the CTE of thin primer is greater than the steel substrate, i.e., $\alpha_c > \alpha_s$, the positive temperature change ($\Delta T > 0$) leads to the opposite direction of residual stress compared to the direction of diffusion stress. This behavior reduces the deflection of coating-substrate system resulting in the compressive residual stress in the coating, allowing the contraction of pre-existing coating microcracks. This shows that compressive residual stress blocks the diffusion of corrosive agents toward the interface and, therefore, avoids corrosion at the interface, measured by corrosion sensors. On the other hand, negative temperature change ($\Delta T < 0$) accounts for the same direction of both the residual and diffusion stresses. This behavior increases the deflection of coating-substrate system and results in tensile residual stress in the coating at a given time. With increasing tensile loading, the coating microcracks open, the crack tips penetrate into the diffusion layer, and the Kirkendall voids then intersect with the crack tip.⁵⁷ After substantial deformation, normally 10%, the macrocracks are visibly wide and their tips, after penetrating through the diffusion layer, arrive at the diffusion layer/substrate interface as shown in Figures 2(a) and (b). This type of crack propagation, normal to the interface, is identified as Mode I path, leading to Type I opening cracks. Widening of these types of microcracks give rise to

unfavorable exposure of the carbon steel substrate. This indicates that tensile residual stress allows the opening of microcracks resulting in the diffusion of corrosive agents, which accelerates the corrosion at the coating/substrate interface as shown in Figure 2.

In the above experimentation, when the coating-substrate system is cooled ($\Delta T < 0$) to the final temperature from its fabrication temperature (318 K [45°C]), tensile residual stress resulting from the mismatch in the coefficients of thermal expansion ($\Delta\alpha = \alpha_s - \alpha_c$) between thin steel substrate and thin primer is evolved. The possible maximum residual stress that can develop in the coating can be determined from Equation (3) as:⁵⁸

$$\sigma_{rc} = E_c \left(1 - \frac{4E_c h}{E_s s} \right) (\alpha_s - \alpha_c) \Delta T \quad (3)$$

The tensile residual stress that is developed in the coating by reducing the temperature (in the second and fourth steps of experimentation) inside the chamber is shown in Figure 3.

Figures 4(a) through (c) show the corrosion current density for all three samples adhered with corrosion sensors. It can be seen that for all three samples during the first step (10 h) when ΔT is equal to 0 ± 1 K, the residual stress was almost zero with no effect on microcracks, resulting in the minimum diffusion of corrosive agents toward the interface. Therefore, corresponding corrosion current density during the first step is negligible for all of the samples, as shown in Figures 4(a) through (c). For the second step (10 h), at point A in Figures 4(a) through (c), ΔT started decreasing such that ΔT reached -15 ± 2 K at about 11 h. This decrease in ΔT resulted in the development of tensile residual stress in the coating causing the opening of microcracks. There was a 3 h lag observed in all of the samples. It is believed that this lag is a result of the diffusion process through the exposed cracks before the corrosion current density starts increasing, indicated as point B in Figures 4(a) through (c). By the time the temperature reached its lowest point during the second step, the corrosion current almost reached its highest point, indicated as point C in Figures 4(a) through (c). During the third step (10 h), when ΔT increased to 0 ± 1 K and maintained for 10 h, a negligible corrosion current density was observed for all of the samples, similar to step 1. For the fourth step, ΔT again started decreasing and reached -7 ± 3 K at about 31 h. It is worth noting that this time there was only a lag of almost 45 min (instead of the previous 3 h) before the corrosion current density started increasing, indicated as point D. The possible reason for this reduced lag at point D during the fourth cycle could be that the coating degradation resulting from accelerated testing with time created new microcracks. These newly developed microcracks, along with the other microcracks, now result in a large diffusion rate of corrosive agents because of the large number of microcracks now opened up when the coating is

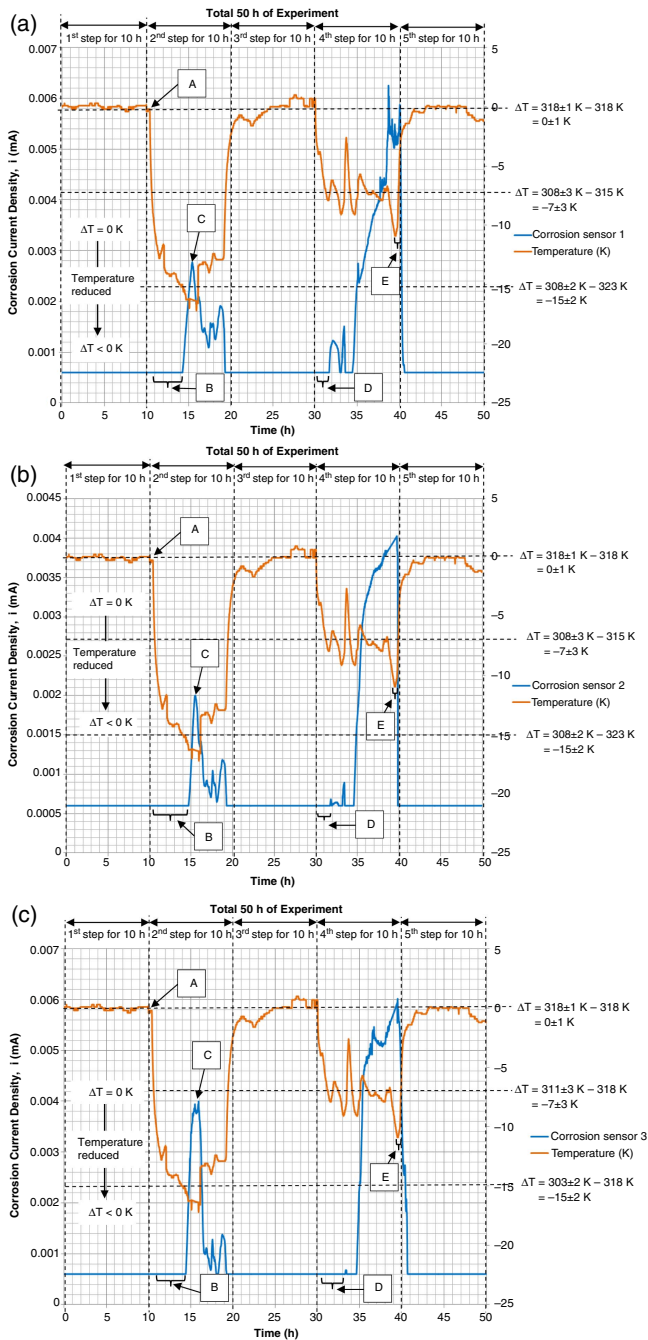


FIGURE 4. Graph showing that, for the case of the second and fourth step (for 10 h) when ΔT is reduced to -7 ± 3 and -15 ± 2 K, this results in the same direction of residual stress gradient as of the diffusion direction. This behavior increases the deflection of coating-substrate system at a given time and results in the evolution of tensile residual stress in the coating. The tensile residual stress opens the pre-existing structural defects in the coating, which allows the corrosive agents to diffuse toward the interface and resulting in the evolution of corrosion current density.

subjected to tensile residual stress at low ΔT . The large diffusion rate resulted in the early corrosion initial-ization, which explains the possible reason for reduced lag time. Likewise, because of the large number of

microcracks and high diffusion rate, high peaks of corrosion current density far greater than the second step were observed, indicated as point E; even at ΔT this time was reduced to -7 ± 3 K, which is lower than the second step. For the fifth step, ΔT increased to 0 ± 1 K and maintained for 10 h with negligible corrosion current density for all of the samples, the same as in steps 1 and 3.

Based on the observation from the 5 step experimentation, a mathematical model has been developed in the next section.

MATHEMATICAL MODEL

A multidisciplinary approach has been adopted during this research to develop a mathematical model. This multidisciplinary technique is unique in terms of combining three distinct fields of material science, solid mechanics, and electrochemistry. A holistic approach to the modeling technique is shown in Figure 5.

Diffusion Model of Coating—Utilization of Material Science Concepts

This part of modeling is specifically developed by considering the diffusion of corrosive species k when the primer coated steel sample is exposed to a corrosive environment. The type and concentration of the species decide the rate of coating delamination. The minimum threshold concentration of the corrosive species is required at the coating defect in order to start the process of delamination.⁵⁹ This part of modeling follows

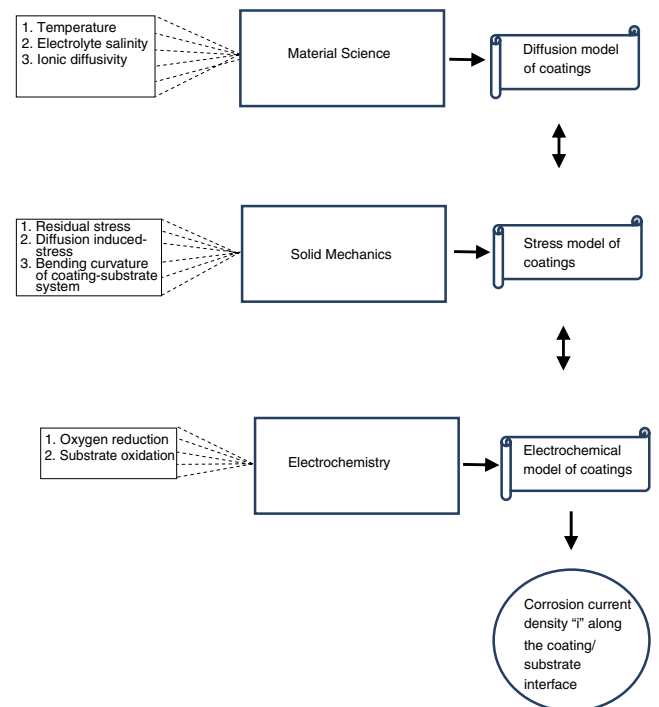


FIGURE 5. Modeling methodology for the developed mathematical model.

the assumptions of: (i) bulk concentration of corrosive species c_{k_B} exists at the defect in coating, and (ii) the electrolyte solution potential Φ follows the electro-neutrality condition at all of the boundaries as:

$$\Phi = \sum_{k=1}^y z_k c_k = 0 \quad (4)$$

where $k = 1, 2 \dots, y$ represents the number of corrosive species involved, and z_k represents the charge number of the species with concentration c_k . The diffusing corrosive species k maintains a concentration c_k over an entire exposed surface of the coating.

The rate of delamination is decided by the concentration of the corrosive species (cation) along the coating/substrate interface, which is found by using a well-known solution of the differential equation for Fick's second law:⁶⁰

$$c_k = c_{k_B} \left[1 - \operatorname{erf} \left(\frac{x}{2\sqrt{D_k t_D}} \right) \right]; \quad c_k = c_{k_B} \quad \text{when} \quad \begin{cases} x=0 \\ t_D > 0 \end{cases} \quad (5)$$

where x defines the distance to the coating defect, t_D is the diffusion time,⁵⁹ and D_k is the average of the standard diffusion coefficient of all of the corrosive species:

$$D_k = [D_{k,STA_{ion}} F_1(T) F_2(RH) F_3(t_{exp})]^{-2} \quad (6)$$

The diffusion coefficient $D_{S,STA_{ion}}$ of each corrosive species along the coating/substrate interface depends upon the temperature (T), pore relative humidity (RH), and time of exposure (t_{exp}). The diffusion coefficient $D_{S,STA_{ion}}$ of the corrosive species along the interface is two orders smaller than in aqueous solution.⁶¹ The terms $F_1(T)$, $F_2(RH)$, and $F_3(t_{exp})$ in Equation (6) are the temperature variation function, RH variation function, and aging function, respectively:⁶²

$$F_1(T) = \exp \left[\left(\frac{G_a}{R} \right) \left(\frac{1}{T_{STA}} - \frac{1}{T} \right) \right] \quad (6a)$$

$$F_2(RH) = \frac{1}{1 + \left(\frac{1-RH}{1-RH_{STA}} \right)^m} \quad (6b)$$

$$F_3(t_{exp}) = \left(\frac{t_{STA}}{t_a} \right)^{n_{ag}} \quad (6c)$$

In Equation (6a), T_{STA} is the standard temperature value, G_a is the activation energy of corrosive species during the diffusion process, and R is the universal gas constant. In Equation (6b), RH is the actual pore relative humidity, RH_{STA} is the standard relative humidity at which D_k drops between maximum and minimum values, and m is the parameter that characterizes the spread of drop in RH_{STA} .⁶⁰ In Equation (6c), t_{STA} is the time of exposure

at which D_k is measured (normally 1 month), t_a is the actual time of exposure, and n_{ag} is the age reduction factor.

The threshold concentration of corrosive species $c_{k_{TH}}$ along the interface to start the process of delamination can be derived from Equation (5) as:

$$c_{k_{TH}} = c_{k_o} \left[1 - \operatorname{erf} \left(\frac{\eta \sqrt{t_p}}{2\sqrt{D_k t_D}} \right) \right] \\ = k_{c_{keq}} c_{k_B} \left[1 - \operatorname{erf} \left(\frac{\eta \sqrt{t_p}}{2\sqrt{D_k t_D}} \right) \right]; \quad t_p = t - t_n \quad (7)$$

where η represents the mobility constant of cations, t represents time passed after the coating defect confronts the electrolyte solution, t_n represents the time required to activate the defect, and c_{k_o} represents the equilibrium concentration of species at the interface in contact with the bulk electrolyte solution c_{k_B} . The equilibrium constant $k_{c_{keq}}$ is used to relate c_{k_o} and c_{k_B} ,

such that $k_{c_{keq}} = \left(\frac{c_{k_o}}{c_{k_B}} \right)$.

For the coating-substrate system exposed to an isotropic electrolyte solution, the chemical potential corresponding to the stressed state of the system can be represented as:⁴²

$$\mu_k^g = \mu_k^o + RT \ln(c_k) - \bar{V}_{P_k} \int_0^{\sigma_m} d\sigma_m; \quad \sigma_m = \frac{1}{3} \int_{i=1}^{i=3} \sigma_i \quad (8)$$

where μ_k^o is the chemical potential in the given standard state, c_k is the concentration of corrosive species derived from Equation (5), and σ_m is the stress tensor and is equal to the mean of the sum of three principle stresses σ_i ($i = 1, 2, \text{ and } 3$), where σ_i can be written as a sum of diffusion-induced stresses σ_{d_i} and residual stresses σ_{r_i} , i.e., $\sigma_i = \sigma_{d_i} + \sigma_{r_i}$. \bar{V}_{P_k} is a scalar term (without the inclusion of stress tensor effect) representing the partial molar volume of diffusing corrosive species k and can be found by using Euler's first theorem for homogeneous functions.⁶⁴

$$\bar{V}_{P_k} = \left(\frac{\partial V_{m_k}}{\partial n_k} \right)_{T,P,n_{k'}} = \left(\frac{V_{m_{k_2}} - V_{m_{k_1}}}{n_{k_2} - n_{k_1}} \right)_{T,P,n_{k'}} \\ = \left(\frac{\frac{m_{k_2}}{\rho_{k_2}} - \frac{m_{k_1}}{\rho_{k_1}}}{n_{k_2} - n_{k_1}} \right)_{T,P,n_{k'}} \quad (9)$$

where \bar{V}_{P_k} depends on the change in molar volume of solution V_{m_k} . The change in molar volume V_{m_k} depends on temperature T , pressure P , and molar concentration of diffusing corrosive species n_k . Consider the case with constant T and P , $V_{m_{k_2}} - V_{m_{k_1}}$ is the change in molar volume corresponding to the change in molar concentration of diffusing species k from n_{k_1} to n_{k_2} .

For the case of an inhomogeneous distribution of solute particles in a non-ideal electrolyte solution, Fick's

second law of diffusion $[\nabla \times \vec{J}_k = -\nabla \times (\frac{D_k c_k}{RT} \mu_k^0)]$,⁶⁵ in conjunction with the law of conservation of mass, can be incorporated with Equations (8) and (9) as:

$$\nabla \times \vec{J}_k = -D_k \nabla^2 c_k + \frac{D_k \bar{V}_{P_k}}{3RT} \nabla c_k \nabla \left[\int_{i=1}^{i=3} (\sigma_{d_i} + \sigma_{r_i}) \right] + \frac{D_k \bar{V}_{P_k}}{3RT} c_k \nabla^2 \left[\int_{i=1}^{i=3} (\sigma_{d_i} + \sigma_{r_i}) \right] \quad (10)$$

where \vec{J}_k is the diffusion flux of corrosive species k and represents the change in concentration of a corrosive species k with respect to time within the stressed coating-substrate system as:

$$\nabla \times \vec{J}_k = -\frac{\partial c_k}{\partial t} \quad (11)$$

Substituting Equation (11) into Equation (10) gives:

$$\frac{\partial c_k}{\partial t} = D_k \nabla^2 c_k - \frac{D_k \bar{V}_{P_k}}{3RT} \nabla c_k \nabla \left[\int_{i=1}^{i=3} (\sigma_{d_i} + \sigma_{r_i}) \right] - \frac{D_k \bar{V}_{P_k}}{3RT} c_k \nabla^2 \left[\int_{i=1}^{i=3} (\sigma_{d_i} + \sigma_{r_i}) \right] \quad (12)$$

Equation (12) follows the law of conservation of mass. It is worth noting that first part of Equation (12) on the right hand side represents the chemical contribution without the inclusion of stress. The second part of the equation includes the contribution of stress along with chemical effects. The third part of equation is the result of stress-induced diffusion.

Stress Model of Coating—Utilization of Solid Mechanics Concepts

This part of modeling is based on solid mechanics concepts integrating the principles of bilayer cantilever beam. In the current research, one layer of the bilayer cantilever beam is considered as coating, while the other layer is considered as substrate. It should be noted that both of the layers of bilayer cantilever exhibit bending as a result of the diffusion-induced stress σ_d and residual stress σ_r . Coating/substrate interface is located at location $x=0$, the free surface of the coating is located at $x=h$, and the free surface of substrate is located at $x=-s$, as shown in Figure 2.

The analysis in this part of modeling is based on the following assumptions: (i) thickness of coating h is very small compared to thickness of substrates, (ii) the material properties of coating and substrate such as Young's modulus, diffusivity, and chemical potential are homogeneous, isotropic, and invariable, (iii) the strain tensor corresponding to principle strains is very small, and (iv) the diffusion-induced

stress σ_d corresponding to time $t=0$ is zero. The diffusion-induced stress evolves after the diffusion of corrosive species k in both layers of cantilever beam at time $t>0$, which results in the bending of beam.

The strain distribution \mathcal{E} in a system is the sum of uniform component \mathcal{E}_{u_j} and a bending component \mathcal{E}_b as:⁵⁸

$$\mathcal{E} = \mathcal{E}_{u_j} + \mathcal{E}_b = \mathcal{E}_{u_j} + \frac{x-t_b}{\zeta_j} \quad (\text{for } -s \leq x \leq h) \quad (13)$$

where $x=t_b$ dictates the neutral point of the bending axis where \mathcal{E}_b is zero and ζ_j represents the radius of curvature of bilayer cantilever. The term $j=r, d$ where r is the residual component and d is diffusion component. Equation (13) will be utilized to derive the relations for residual stresses σ_r and diffusion-induced stresses σ_d in a bilayer cantilever beam. This equation is analogous to the strain continuity equation in the Timoshenko shear model.⁶⁶

The relation for the residual stresses in a bilayer cantilever beam is given as:⁴²

$$\sigma_{r_c} = E_c \left(\mathcal{E}_{u_r} + \frac{x-t_b}{\zeta_r} - \alpha_c \Delta T \right) \quad (14a)$$

$$\sigma_{r_s} = E_s \left(\mathcal{E}_{u_r} + \frac{x-t_b}{\zeta_r} - \alpha_s \Delta T \right) \quad (14b)$$

where E_c , E_s , α_c , and α_s are the elastic moduli and coefficient of thermal expansion (CTE) of coating and substrate, respectively, and ΔT is the change in temperature from fabrication temperature or during application. The terms \mathcal{E}_{u_r} , t_b , and $1/\zeta_r$ can be expanded as:⁶⁷

$$\mathcal{E}_{u_r} = \frac{(E_s \alpha_s s + E_c \alpha_c h) \Delta T}{(E_s s + E_c h)} \quad (15a)$$

$$t_b = \frac{-E_s s^2 + E_c h^2}{2(E_s s + E_c h)} \quad (15b)$$

$$\frac{1}{\zeta_r} = \frac{3[E_s s^2 (\mathcal{E}_{u_r} - \alpha_s \Delta T) - E_c h^2 (\mathcal{E}_{u_r} - \alpha_c \Delta T)]}{E_s s^2 (2s + 3t_b) + E_c h^2 (2h - 3t_b)} \quad (15c)$$

The average diffusion-induced stresses distribution in a bilayer cantilever beam are related to strains by using a modified form of stress-strain relation as:

$$\sigma_{d_c} = E_c \left(\mathcal{E}_{u_d} + \frac{x-t_b}{\zeta_d} - \frac{1}{3} c_{k_c} \bar{V}_{P_{k_c}} \right) \quad (16a)$$

$$\sigma_{d_s} = E_s \left(\mathcal{E}_{u_d} + \frac{x-t_b}{\zeta_d} - \frac{1}{3} c_{k_s} \bar{V}_{P_{k_s}} \right) \quad (16b)$$

The bi-axial strains are identical along y and z planes for the case of planar geometry; therefore, E_m can be replaced by $E_m/(1-\nu_m)$, where ν_m is the Poisson's ratio

and $m = c, s$. The equations for the diffusion-induced stresses (Equations [16a] and [b]) are similar to the equations for the residual stresses (Equations [14a] and [b]). However, for diffusion processes, the coating properties may be assumed to change linearly⁶⁸ with the concentration of diffusing corrosive species k , which results in diffusion-induced stresses. Therefore, it is possible to calculate diffusion-induced stresses by analogy to thermal stresses, which has been previously calculated by Prussin⁶⁹ and Zhang.⁷⁰ Prussin and Zhang treated concentration gradients c_{k_c} analogous to those generated by temperature gradients ΔT and partial molar volume \bar{V}_{P_k} analogous to thermal expansion α .

The strain and stress distribution in bilayer cantilever beam (Equations [13], [16a], and [16b]) resulting from diffusion are dependent on the solution of two parameters, i.e., ε_{u_d} and $1/\zeta_d$. It is possible to find ε_{u_d} and $1/\zeta_d$ by using the following two boundary conditions.

At first, the resultant force corresponding to uniform strain component is zero, such that:

$$\int_{Z_c} E_c \left(\varepsilon_{u_d} - \frac{1}{3} \bar{V}_{P_{k_c}} c_{k_c} \right) dZ_c + \int_{Z_s} E_s \left(\varepsilon_{u_d} - \frac{1}{3} \bar{V}_{P_{k_s}} c_{k_s} \right) dZ_s = 0 \quad (17)$$

The terms $Z_c = bh$, $Z_s = bs$, and $b = b_s = b_h$. The solution of Equation (17) gives:

$$\varepsilon_{u_d} = \frac{1}{3} \left(\frac{E_c h \bar{V}_{P_{k_c}} \bar{c}_{k_c} + E_s s \bar{V}_{P_{k_s}} \bar{c}_{k_s}}{E_c h + E_s s} \right) \quad (18)$$

where $\bar{c}_{k_c} = \frac{1}{h} \int_0^h c_{k_c} dx$ and $\bar{c}_{k_s} = \frac{1}{s} \int_{-s}^0 c_{k_s} dx$.

Second, the summation of bending moments of cantilever layers with respect to neutral point, i.e., $x = t_b$ is zero, such that:

$$\int_{Z_c} \sigma_{d_c}(x - t_b) dZ_c + \int_{Z_s} \sigma_{d_s}(x - t_b) dZ_s = 0 \quad (19)$$

The bending curvature of cantilever layers $1/\zeta_d$ resulting from diffusion-induced stress can be determined from the solution of Equations (13), (16a), (16b), (18), and (19):

$$\frac{1}{\zeta_d} = \frac{2[E_c E_s h s (2s)(\bar{V}_{P_{k_c}} c_{k_c} - \bar{V}_{P_{k_s}} c_{k_s})]}{E_c^2 h^4 + E_s^2 s^4 + 2E_c E_s h s (2h^2 + 3hs + 2s^2)} \quad (20)$$

Substituting the residual stresses Equations (14a) and (b) and diffusion-induced stresses Equations (16a) and (b) into Equation (12) forms a *coupling relationship* between stress model of cantilever layers and diffusion

model as:

$$\frac{\partial c_{k_c}}{\partial t} = D_{k_c} \left(1 + \frac{E_c \bar{V}_{P_{k_c}}}{9RT} c_{k_c} \right) \frac{\partial^2 c_{k_c}}{\partial x^2} + D_{k_c} \frac{E_c \bar{V}_{P_{k_c}}}{9RT} \left(\frac{\partial c_{k_c}}{\partial x} \right)^2 - \frac{D_{k_c} E_c \bar{V}_{P_{k_c}}}{3RT} \frac{\partial c_{k_c}}{\partial x} \left(\frac{1}{\zeta_d} + \frac{1}{\zeta_r} \right) \quad (21a)$$

$$\frac{\partial c_{k_s}}{\partial t} = D_{k_s} \left(1 + \frac{E_s \bar{V}_{P_{k_s}}}{9RT} c_{k_s} \right) \frac{\partial^2 c_{k_s}}{\partial x^2} + D_{k_s} \frac{E_s \bar{V}_{P_{k_s}}}{9RT} \left(\frac{\partial c_{k_s}}{\partial x} \right)^2 - \frac{D_{k_s} E_s \bar{V}_{P_{k_s}}}{3RT} \frac{\partial c_{k_s}}{\partial x} \left(\frac{1}{\zeta_d} + \frac{1}{\zeta_r} \right) \quad (21b)$$

In Equations (21a) and (b), in the third part on right hand side, the terms can be written as: $\frac{E_c}{\zeta_d} = \frac{\partial \sigma_{d_c}}{\partial t}$, $\frac{E_c}{\zeta_r} = \frac{\partial \sigma_{r_c}}{\partial x}$, $\frac{E_s}{\zeta_d} = \frac{\partial \sigma_{d_s}}{\partial t}$, and $\frac{E_s}{\zeta_r} = \frac{\partial \sigma_{r_s}}{\partial x}$, where $\frac{\partial \sigma_{d_c}}{\partial t}$ and $\frac{\partial \sigma_{r_c}}{\partial x}$, and $\frac{\partial \sigma_{d_s}}{\partial t}$ and $\frac{\partial \sigma_{r_s}}{\partial x}$ represent the rate of change of diffusion-induced stresses and residual stresses in coating and substrate, respectively.

The total bending curvature of cantilever layers $\left(\frac{1}{\zeta_d} + \frac{1}{\zeta_r} \right)$ in Equations (21a) and (b) as a result of the diffusion-induced stress and residual stress can be written as the summation of Equations (15c) and (20):

$$\frac{1}{\zeta_d} + \frac{1}{\zeta_r} = \frac{2[E_c E_s h s (2s)(\bar{V}_{P_{k_c}} c_{k_c} - \bar{V}_{P_{k_s}} c_{k_s})]}{E_c^2 h^4 + E_s^2 s^4 + 2E_c E_s h s (2h^2 + 3hs + 2s^2)} + \frac{3[E_s s^2 (\varepsilon_u - \alpha_s \Delta T) - E_c h^2 (\varepsilon_u - \alpha_c \Delta T)]}{E_s s^2 (2s + 3t_b) + E_c h^2 (2h - 3t_b)} \quad (22)$$

Equation (22) shows that the total bending curvature of cantilever layers is the sum of bending curvature of cantilever layers resulting from diffusion-induced stress $1/\zeta_d$ and bending curvature of cantilever layers resulting from residual stress $1/\zeta_r$. The bending curvatures as a result of diffusion-induced stress and residual stress are dependent upon the concentration of corrosive species c_k and CTE mismatch resulting from temperature change ΔT , respectively.

Electrochemical Model of Coating—Utilization of Electrochemistry Concepts

This part of modeling gives the design for corrosion current density resulting from the electrochemical reactions along coating/substrate interface. The corrosion current density depends on the electrochemical reactions as a result of substrate dissolution and oxygen reduction. The conventional equation of corrosion current density from literature⁷¹⁻⁷² can now be incorporated with the derived equation of total bending curvature [Equation [22]]. This indicates that the electrochemical reactions along the coating/substrate interface also depend on the total bending curvature resulting from diffusion-induced stress ($1/\zeta_d$)

and residual stress ($1/\zeta_r$). No homogeneous reactions are taken into account; only electrochemical reactions are considered. The expressions of the polarization kinetics for oxygen reduction and substrate dissolution are developed, which are presented next.

The polarization kinetics for the reaction involving oxygen reduction is expressed as: $O_2 + 2H_2O + 4e^- \rightarrow 4OH^-$.

By incorporating the total bending curvature $\frac{1}{\zeta_d} + \frac{1}{\zeta_r}$ derived in Equation (22) with the conventional equation of corrosion current density,⁷¹⁻⁷² a new equation has been developed for the current density resulting from the oxygen reduction at any position along the coating/substrate interface:

$$i_{O_2}^{coat} = - \left(\frac{1}{-nFD_{O_2}c_{O_2} \left(\frac{\left(\frac{1}{\zeta_d} + \frac{1}{\zeta_r}\right) \left(\frac{1}{\zeta_{dnd}} + \frac{1}{\zeta_{rnd}}\right)}{\left(\frac{1}{\zeta_d} + \frac{1}{\zeta_r}\right) h_{nd} + \left(\frac{1}{\zeta_{dnd}} + \frac{1}{\zeta_{rnd}}\right) h_d} \right)} - 10^{\frac{V-E_{O_2}^0}{\beta_{O_2}}} \right)^{-1};$$

$$V = E - \Phi \quad (23)$$

where $E_{O_2}^0$, E , Φ , and β_{O_2} are the equilibrium potential of oxygen, substrate potential, solution potential, and oxygen Tafel slope, respectively. The terms h_d and h_{nd} are the coating thickness for delaminated and nondelaminated coating, respectively. The terms $\frac{1}{\zeta_{dnd}}$ and $\frac{1}{\zeta_{rnd}}$, and $\frac{1}{\zeta_{rd}}$ and $\frac{1}{\zeta_{rd}}$ are the bending curvatures resulting from diffusion-induced stress and residual stress for delaminated and nondelaminated coating-substrate system, respectively. The term c_{O_2} represents the dissolved concentration of oxygen at coating surface, D_{O_2} is the diffusion coefficients for oxygen, and n is the number of electrons transferred.⁷³

The polarization kinetics for the forward reaction involving substrate dissolution is expressed as: $S \rightarrow S^{n+} + ne^-$

The current density i^s at the coating/substrate interface as a result of substrate dissolution is given as:⁶³

$$i^s = i_{o,s} 10^{\frac{V-E_s^0}{\beta_s}}; \quad V = E - \Phi \quad (24)$$

where E_s^0 , β_s , and $i_{o,s}$ are the equilibrium potential of substrate, substrate-Tafel slope, and exchange current density for the substrate dissolution reaction, respectively.

The equations ([23] and [24]) for both the oxygen reduction and substrate dissolution can be combined to generate the net corrosion current density "i" along the coating/substrate interface as:

$$i = i_{O_2}^{coat} + i^s \quad (25)$$

It is clear that the above equation agrees with Allahar,⁷² when the total bending curvature $\left(\frac{1}{\zeta_d} + \frac{1}{\zeta_r}\right)$ resulting from diffusion-induced stress and residual

stress is replaced by interface porosity (gap at the interface between coating and substrate) $p^{1.5}$ in a coating-substrate system.

IMPLEMENTATION OF MATHEMATICAL MODEL

The initial and boundary conditions for the stressed bilayer cantilever are expressed as follows:

$$c_{k_c}(x) = c_{k_s}(x) = 0 \quad \text{at time } t=0 \quad (26)$$

$$\left. \frac{\partial c_{k_s}}{\partial x} \right|_{x=s} = 0; \quad c_{k_c}(h) = c_{k_o} \quad \text{at time } t > 0 \quad (27)$$

For numerical simulation work, all of the parameters and variables, which are used in the equations, should be converted in to dimensionless forms as:

$$D'_k = D_{k_c}/D_{k_s}; \quad D'_{O_2} = D_{O_2}/D_{O_{2o}} \quad (28a)$$

$$x' = \frac{x}{b} = \frac{x}{h+s} \quad (28b)$$

$$c'_{k_c} = c_{k_c}/c_{k_o}; \quad c'_{k_s} = c_{k_s}/c_{k_o}; \quad c'_{O_2} = c_{O_2}/c_{O_{2o}} \quad (28c)$$

$$\overline{V}_{P_{k_c}} = \overline{V}_{P_{k_s}} = 1 \quad (28d)$$

$$t' = D_{k_c} t/h^2 \quad (28e)$$

$$\frac{1}{\zeta'_r} = \frac{h}{\zeta_r} \frac{2E_c \overline{V}_{P_k}}{3RT} = \frac{4\Lambda^{-1} \left(\frac{1}{\eta}\right) \left(1 + \frac{1}{\eta}\right)^2 (\alpha_c - \alpha_s) \Delta TE_c \overline{V}_{P_k}}{\left(\Lambda^{-1} \left(\frac{1}{\eta}\right)^2 - 1\right)^2 + 4\Lambda^{-1} \frac{1}{\eta} \left(\frac{1}{\eta} + 1\right)^2} RT \quad (28f)$$

$$\frac{1}{\zeta'_d} = \frac{b}{\zeta_d \overline{V}_{P_k} c_{k_o}} = \frac{4(1+1/\eta)^3 [1 + (\Lambda^{-1}/\eta)] \left(\Lambda^{-1} \int_{-\frac{1/\eta}{1/\eta+1}}^0 c'_{k_s} x' dx' + \int_0^{\frac{1}{1/\eta+1}} c'_{k_c} x' dx' \right)}{\left[\Lambda^{-1} \left(\frac{1}{\eta}\right)^2 - 1 \right]^2 + 4\Lambda^{-1} \left(\frac{1}{\eta}\right) \left(\frac{1}{\eta} + 1\right)^2} = \frac{2 \left[1 - \Lambda^{-1} \left(\frac{1}{\eta}\right)^2 \right] \left(1 + \frac{1}{\eta}\right)^2 \left(\Lambda^{-1} \int_{-\frac{1/\eta}{1/\eta+1}}^0 c'_{k_s} x' dx' + \int_0^{\frac{1}{1/\eta+1}} c'_{k_c} x' dx' \right)}{\left[\Lambda^{-1} \left(\frac{1}{\eta}\right)^2 - 1 \right]^2 + 4\Lambda^{-1} \left(\frac{1}{\eta}\right) \left(\frac{1}{\eta} + 1\right)^2} \quad (28g)$$

$$i' = i_{O_2}^{coat'} + i^{s'} = - \left\{ \frac{1}{-D'_{O_2} c'_{O_2} \left[\frac{\left(\frac{1}{\zeta'_d} + \frac{1}{\zeta'_r}\right) \left(\frac{1}{\zeta'_{dnd}} + \frac{1}{\zeta'_{rnd}}\right)}{\left(\frac{1}{\zeta'_d} + \frac{1}{\zeta'_r}\right) \frac{h_{nd}}{s} + \left(\frac{1}{\zeta'_{dnd}} + \frac{1}{\zeta'_{rnd}}\right) \frac{h_d}{s} \right]} - 10^{\frac{V-E_{O_2}^0}{\beta_{O_2}}} \right\}^{-1} + 10^{\frac{V-E_s^0}{\beta_s}} \frac{i_{o,s}}{i_{o,s_o}} \quad (28h)$$

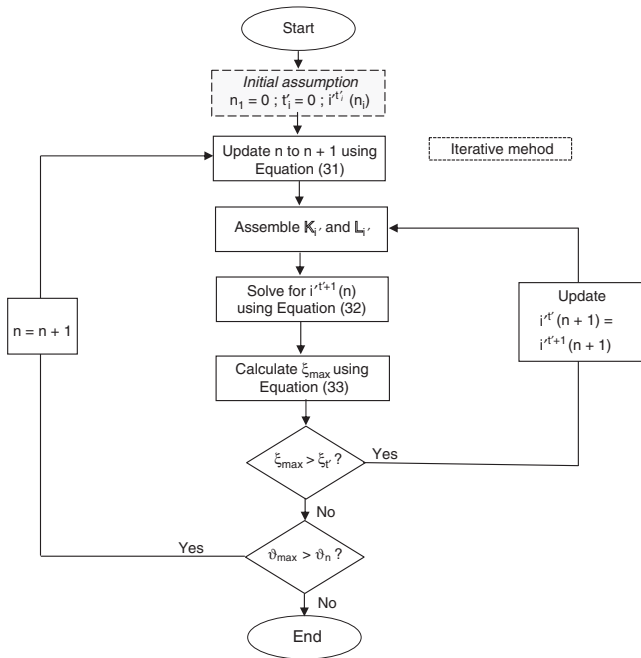


FIGURE 6. Newly developed algorithm utilizing Newton-Raphson method in order to solve and implement the mathematical model.

where $\Lambda^{-1} = E_c/E_s$ and $1/\eta = h/s$, and it is assumed that $\bar{V}_{pk} = \bar{V}_{pkc} = \bar{V}_{pks}$.

The dimensionless partial differential equation (PDE) Equation (28h) is then solved by developing a generalized Equation (23) representing the time-iterative algorithm shown in Figure 6.

$$\frac{\partial i'}{\partial t}(n) = i'^{t'}(n) \quad (29)$$

Temperature ΔT influences the “time discretization” of “i” during the application of coating-substrate system. The iterations of parameter ΔT is represented by “n” and the time states are represented by superscript “t’” which is generalized in Equation 29. Newton-Raphson method⁷⁴ is utilized to solve the time-varying PDE $\frac{\partial i'}{\partial t}$. The governing PDE $\frac{\partial i'}{\partial t}$ for normalized corrosion current density i' in the domain is discretized in time and space, and cast into the matrix form by using Newton-Raphson method.

The algorithm follows the following steps.

- (i) The algorithm initiates the iterative process for a parameter and computes Δn as:

$$\Delta n = n - n_i \quad \text{where } n_i = 0 \quad (30)$$

- (ii) The initially calculated Δn in Equation (24) is used every time to upgrade n to $n + 1$ by using:

$$n + 1 = n + \Delta n \quad (31)$$

- (iii) The value of $i'^{t'}$ (n) at time $t'_1 = 0$ is assumed as $i'^0(n)$. This is in accordance with the boundary condition in stressed cantilever, as mentioned in Equation (26).
- (iv) The algorithm then performs the time discretization of i' which is then cast into the matrix form as:

$$\mathbb{K}_{i'} \cdot i'^{t'+1}(n_i) = \mathbb{L}_{i'} \quad (32)$$

where $\mathbb{K}_{i'}$ represents the coefficient matrix which is a function of $i'^{t'+1}$ at time state $t' + 1$. The vector $\mathbb{L}_{i'}$ is the load vector which is a function of $i'^{t'}$ (n) at time state t' . Both of the matrices $\mathbb{K}_{i'}$ and $\mathbb{L}_{i'}$ are used in the computation of the value of $i'^{t'+1}$.

- (v) The time convergence criterion $\xi_{t'}$ is calculated as:

$$\xi_{t'} = 100 \left(\frac{f^{t'+1} - f^{t'}}{f^{t'}} \right) \quad (33)$$

where f is a generic term representing time t' . The value of f for each time state in the domain, excluding that on the boundary conditions, was computed and the maximum value of ξ_{\max} was determined. On the comparison of ξ_{\max} with $\xi_{t'}$, if $\xi_{\max} > \xi_{t'}$, the value of t' is updated, and control returned to step (iv). For the condition $\xi_{\max} < \xi_{t'}$, the algorithm moves to next step.

- (vi) The convergence criterion ϑ_n for variable parameter n is calculated as:

$$\vartheta_n = 100 \left(\frac{m^{n+1} - m^n}{m^n} \right) \quad (34)$$

where m is a generic term representing variable parameter n . The value of n is updated for the condition if $\vartheta_{\max} > \vartheta_n$ by returning the control to step (ii). For the condition $\vartheta_{\max} < \vartheta_n$, the algorithm ends.

RESULTS AND DISCUSSION

Based on the numerical simulation by using Newton-Raphson method, the effect of residual stress gradient $1/\zeta'_r$ (resulting from the change in temperature ΔT) on corrosion current density is discussed in this section.

The corrosion current density is significantly affected by the residual stress and diffusion-induced stress. Figure 7 illustrates the evolution of normalized corrosion current density incorporating the effects of diffusion-induced gradient $1/\zeta'_{sd}$ and residual stress gradient $1/\zeta'_r$ of the coating. It is clear that the normalized corrosion current density depends upon the diffusion of corrosive agents through the coating microcracks, which accounts

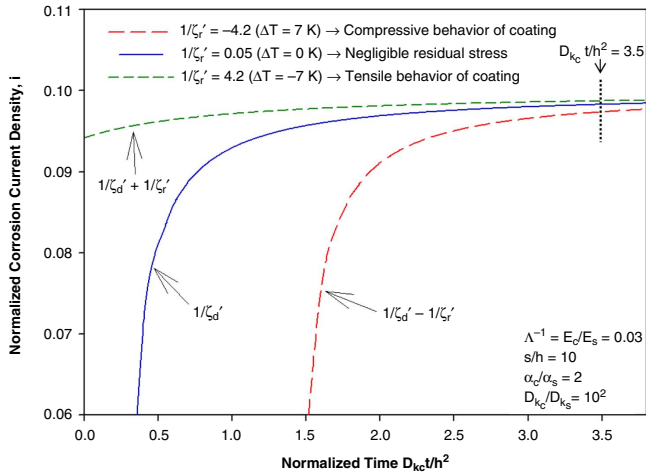


FIGURE 7. Figure illustrating the evolution of normalized corrosion current density “*i*” incorporating the effects of diffusion-induced gradient $1/\zeta'_d$ and residual stress gradient $1/\zeta'_r$ of the coating. The residual stress $1/\zeta'_r$ in the coating could be compressive (when $\Delta T = 7\text{ K} [> 0]$) and could be tensile (when $\Delta T = -7\text{ K} [< 0]$).

for the diffusion-induced gradient $1/\zeta'_d$. However, the diffusion-induced gradient $1/\zeta'_d$ is changed by the residual stress gradient depending upon the mismatch in CTE of coating and substrate. Because the CTE of the coating is twice that of the substrate, i.e., $\alpha_c = 2\alpha_s$, therefore, the positive temperature change $\Delta T = 7\text{ K} (> 0)$ leads to the opposite direction of residual stress ($1/\zeta'_r = -4.2$) compared to the diffusion stress direction. Thus, the total gradient can be written as: $1/\zeta'_d - 1/\zeta'_r$. This type of stress gradient results in the evolution of the compressive residual stress at a given time, as shown in Figure 7. The compressive behavior of the coating constricts the pre-existing coating microcracks, which in turn creates obstacles for the diffusion of corrosive agents and reduces the corrosion current density at the interface. On the other hand, the negative temperature change $\Delta T = -7\text{ K} (< 0)$ leads to the same direction of both the stresses, i.e., residual stress ($1/\zeta'_r = 4.2$) and diffusion stress. Thus, the total gradient can be written as: $1/\zeta'_d + 1/\zeta'_r$. This type of stress gradient results in the evolution of the tensile residual stress. The tensile behavior opens the pre-existing coating microcracks and allows the diffusion of corrosive agents before reaching the saturation state of corrosive agents in the coating. This results in the increase of corrosion current density. The results indicate that a 14° change in temperature can result in a 100% shift in the corrosion current density at a given diffusing time. For the case when $\Delta T = 0\text{ K}$, the effect of residual stress gradient $1/\zeta'_r$ is negligible: only the diffusion-induced gradient $1/\zeta'_d$ influences the corrosion current density. This indicates that the residual stress plays a vital role in the corrosion current density; however, the effects of residual stress

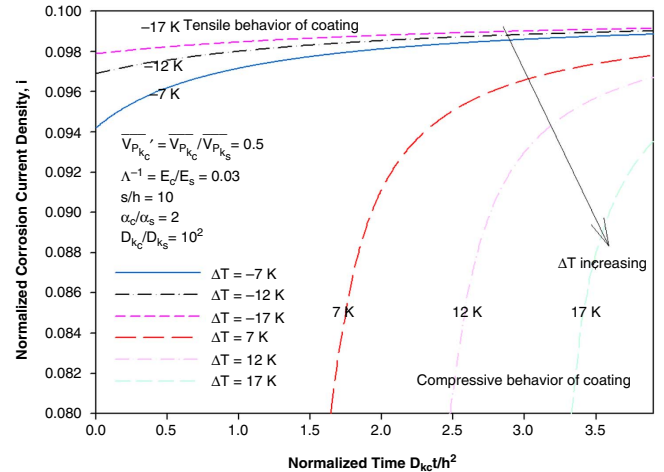


FIGURE 8. Figure showing the effects of various temperature values ΔT on the corrosion current density “*i*.” It is clear that as the temperature increases from $\Delta T = -17\text{ K}$ (tensile behavior of coating) to $\Delta T = 17\text{ K}$ (compressive behavior of coating), the corrosion current density decreases.

on the corrosion current density gradually disappear when the saturation condition of corrosive agents is reached. From Figure 7 it can be seen that for the coating under tensile behavior $\Delta T = -7\text{ K}$, the saturation condition is reached well before $D_{kc}t/h^2 = 3.5$; however, for coating under compressive behavior $\Delta T = 7\text{ K}$, the saturation condition is reached at some point in time after $D_{kc}t/h^2 = 3.5$.

Effects of various temperature values ΔT on the corrosion current density are shown in Figure 8, where $\bar{V}_{P_{kc}}' = \bar{V}_{P_{kc}}/\bar{V}_{P_{ks}} = 0.5$, $\Lambda^{-1} = E_c/E_s = 0.03$, $s/h = 10$, $\alpha_c/\alpha_s = 2$, and $D_{kc}/D_{ks} = 10^2$. From Figure 8, it is clear that as the temperature increases from $\Delta T = -17\text{ K}$ to $\Delta T = -7\text{ K}$ (tensile regime), the corrosion current density decreases. However, this decrease in the corrosion current density is observed only for a time period of $D_{kc}t/h^2 < 3.5$. After this time period, the saturation condition of corrosive agents is reached and the corrosion current density becomes independent of the change in temperature ΔT . For the increase in temperature from $\Delta T = 7\text{ K}$ to $\Delta T = 17\text{ K}$ (compressive regime), the corrosion current density still decreases but the saturation condition of corrosive agents is reached at some point after time $D_{kc}t/h^2 = 3.5$. This saturation behavior of corrosive agents in compressive regime shows that the saturation time is higher when the coating is subjected to compressive residual stress. In conclusion, the residual stress plays a vital role only at the start of exposure; however, the effect of residual stress disappears when the saturation is reached.

Figure 9 shows the evolution of corrosion current density corresponding to various values of moduli ratio E_c/E_s , and the residual stress gradient $1/\zeta'_r$ at two

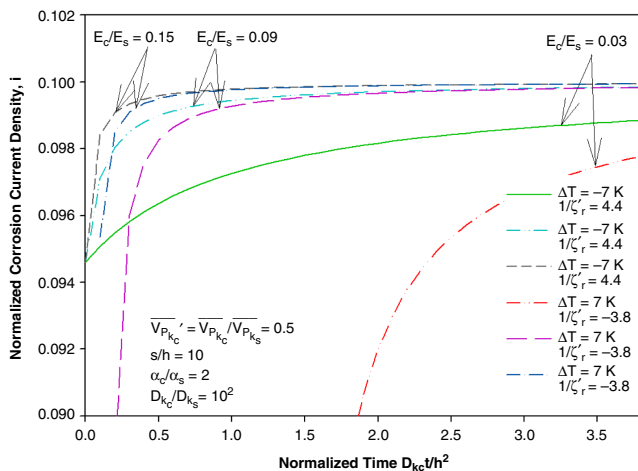


FIGURE 9. Figure showing the evolution of corrosion current density “*i*” corresponding to various values of moduli ratio E_c/E_s and the residual stress gradient $1/\zeta'_r$ at two different temperatures, i.e., $\Delta T = -7$ K and $\Delta T = 7$ K. The corrosion current density increases with the increase in the ratios of modulus, E_c/E_s . This indicates that increasing the flexibility of substrate can increase the corrosion current density.

different temperatures, i.e., $\Delta T = -7$ K and $\Delta T = 7$ K. The parameters are set as $\overline{V_{P_{kc}}}' = \overline{V_{P_{kc}}}/\overline{V_{P_{ks}}} = 0.5$, $s/h = 10$, $\alpha_c/\alpha_s = 2$, and $D_{kc}/D_{ks} = 10^2$. It is clear in Figure 9 that the corrosion current density gradually increases and then stabilizes with the increasing time for various ratios of moduli. It is worth noting, that the corrosion current density increases with the increase in the ratios of modulus, E_c/E_s . This indicates that, for a given value of thickness h/s and concentration of corrosive species, increasing the flexibility of substrate can increase the corrosion current density. It is also clear that the corrosion current density increases or decreases with the magnitude of residual stress gradient $1/\zeta'_r$. The negative temperature change ($\Delta T = -7$ K) accounts for the increase in total gradient ($1/\zeta'_d + 1/\zeta'_r$) because of the same direction of residual stress and the diffusion stress. This behavior in turn increases in the corrosion current density. However, the positive temperature change ($\Delta T = 7$ K) accounts for the decrease in total gradient ($1/\zeta'_d - 1/\zeta'_r$), which in turn decreases in the corrosion current density.

For the case considering the total thickness to be constant, the effects of thickness ratio s/h on corrosion current density are shown in Figure 10, where $\overline{V_{P_{kc}}}' = \overline{V_{P_{kc}}}/\overline{V_{P_{ks}}} = 0.5$, $\Delta^{-1} = E_c/E_s = 0.03$, $\alpha_c/\alpha_s = 2$, and $D_{kc}/D_{ks} = 10^2$. From Figure 10, it is observed that when $\Delta T < 0$ K under tensile condition, the corrosion current density decreases for the thickness ratio $s/h < 4.5$, and then becomes stable for $s/h > 4.5$. This clearly indicates that the tensile residual stress in coating assists the opening of coating microcracks only if the thickness ratio s/h is less than 4.5. However,

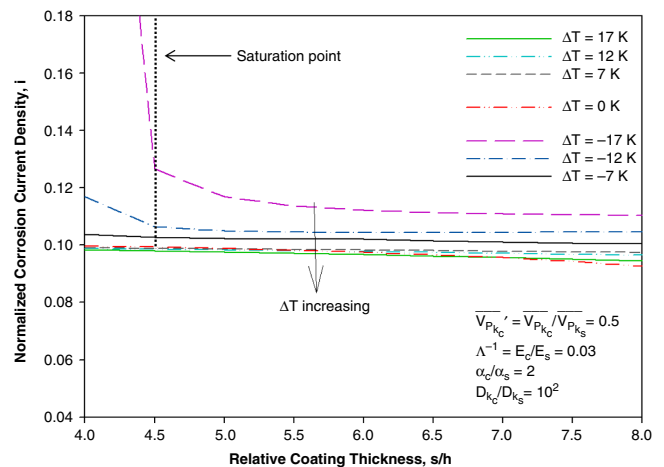


FIGURE 10. Figure showing the effects of relative thickness s/h on corrosion current “*i*” density. It is observed that when $\Delta T < 0$ K under tensile condition, the corrosion current density decreases for the thickness ratio $s/h < 4.5$, and then becomes stable for $s/h > 4.5$. For the case of compressive residual stress when $\Delta T > 0$ K, the thickness ratio s/h does not have a significant effect and results in constant corrosion current density for all thickness ratios s/h .

when the thickness ratio s/h exceeds 4.5 (i.e., for thin coatings), microcracks opening is no longer influenced by tensile residual stress in the coating. On the other hand, for the case of compressive residual stress when $\Delta T > 0$ K, the thickness ratio s/h does not significantly affect the microcracks and therefore results in constant corrosion current density for all thickness ratios s/h . It can be concluded that the thickness ratio plays a significant role in controlling corrosion current density only if the coating is under tensile residual effect, while if the coating is under compressive residual effect, the thickness ratio s/h does not affect the corrosion current density. It is also clear from Figure 11 that for the condition $\Delta T = 7$ K, when the coating is under compression, the corrosion current density is independent of time $D_{kc}t/h^2$ for any ratio of thickness s/h .

Figure 12 illustrates the evolution of corrosion current density involving the effects of CTE mismatch between coating and substrate. For a qualitative discussion two modulus ratios have been considered (i) when $\Delta^{-1} = E_c/E_s = 0.2$ and (ii) when $\Delta^{-1} = E_c/E_s = 0.03$. Now considering the first case with $\Delta^{-1} = E_c/E_s = 0.2$, it is clear from Figure 12(a) that for the condition, when $\Delta T = -7$ K, the corrosion current density increases with the decrease in the CTE mismatch between coating and substrate. For instance, considering $\Delta T = -7$ K, for the case when $\alpha_c/\alpha_s = 2$, the corrosion current density is higher than the corrosion current density for $\alpha_c/\alpha_s = 10$ and $\alpha_c/\alpha_s = 50$. This behavior is a result of the residual stress gradient $1/\zeta'_r$, which decreases with the increase in α_c/α_s , and thus, results in the decrease of

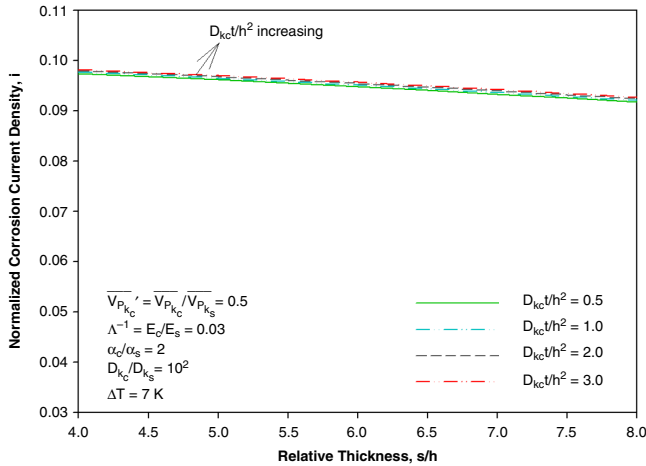


FIGURE 11. Figure showing the corrosion current density “ i ” for various values of time $D_{kc}t/h^2$ by considering temperature $\Delta T = 7$ K. It is clear that when the coating is under compression, the corrosion current density is independent of time $D_{kc}t/h^2$ for any ratio of thickness s/h .

total stress gradient $1/\zeta'_d + 1/\zeta'_r$. This decrease in the total stress gradient results in the decrease of corrosion current density. However, for $\Delta T = 7$ K, the corrosion current density is low for smaller CTE mismatch, i.e., the corrosion current density for $\alpha_c/\alpha_s = 2$ is lower than the corrosion current density for $\alpha_c/\alpha_s = 10$ and $\alpha_c/\alpha_s = 50$. This behavior is a result of the residual stress gradient $1/\zeta'_r$, which increases with the increase in α_c/α_s , and thus, results in the increase of total stress gradient $1/\zeta'_d - 1/\zeta'_r$. This increase in the total stress gradient results in the increase of corrosion current density.

Now considering the second case with modulus ratio $\Lambda^{-1} = E_c/E_s = 0.03$, it is clear that when $\Delta T = -7$ K, behavior similar to the previous case (when $\Lambda^{-1} = E_c/E_s = 0.2$) was again observed in which the corrosion current density was high for small CTE mismatch and was low for large CTE mismatch, as shown in Figure 12(b). For $\Delta T = 7$ K, the behavior of corrosion current density was again similar to the previous case.

However, the notable difference between both of these cases was that the values of corrosion current density corresponding to all of the CTE mismatches (α_c/α_s equal to 50, 10, and 2) were found to be higher for larger modulus ratio (e.g., $E_c/E_s = 0.2$) in the first case compared to the smaller modulus ratio (e.g., $E_c/E_s = 0.03$) in the second case. The reason behind this behavior is that for a given ΔT , thickness, and concentration of diffusion species, higher flexibility of substrate (smaller E_s), as in case 1, can increase the deflection of coating-substrate system. This behavior can result in the evolution of higher tensile residual stress in the coating, allowing the microcracks to open up wide, resulting in higher corrosion current density. On the other hand, lower flexibility of

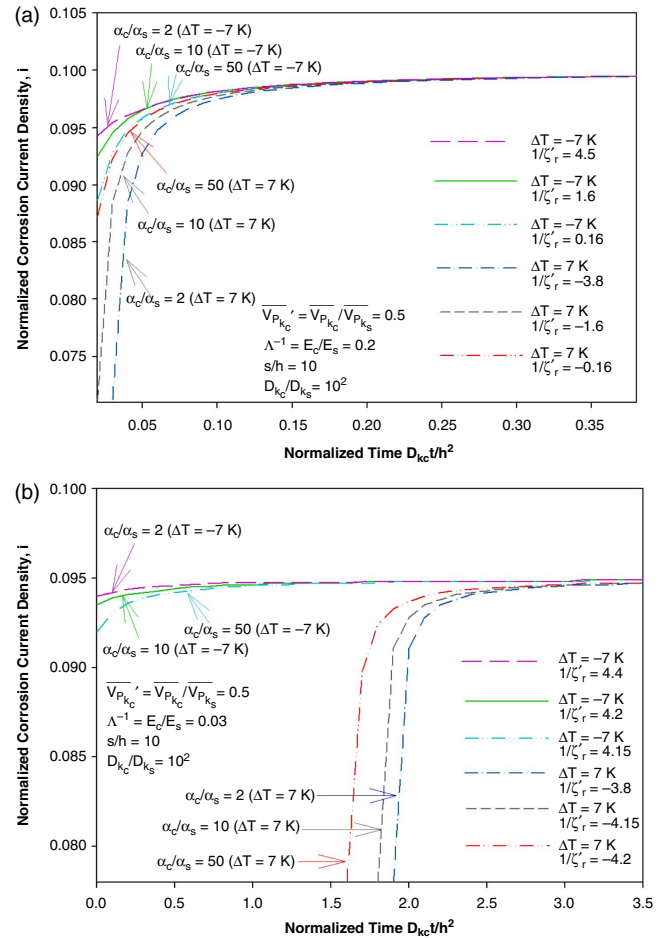


FIGURE 12. Figure showing the evolution of corrosion current density “ i ” involving the effects of CTE mismatch between coating and substrate for two cases (a) when $\Delta^{-1} = E_c/E_s = 0.2$, and (b) when $\Delta^{-1} = E_c/E_s = 0.03$. For the case when $E_c/E_s = 0.2$, higher modulus ratio accounts for larger corrosion current density compared to lower modulus ratio $E_c/E_s = 0.03$. However, for a given modulus ratio, larger corrosion current density can be avoided if higher Δ_c/Δ_s is used for the applications with negative temperature change ($\Delta T < 0$) and lower Δ_c/Δ_s is used for the applications with positive temperature change ($\Delta T > 0$).

substrate (higher E_s), as in case 2, can decrease the deflection of coating-substrate system. This behavior can result in the evolution of smaller tensile residual stress in the coating opening microcracks that are not wide enough, resulting in lower corrosion current density.

Therefore, it can be concluded that for coating-substrate system, higher modulus ratio accounts for larger corrosion current density compared to lower modulus ratio. However, for a given modulus ratio, larger corrosion current density can be avoided if higher α_c/α_s is used for the applications with negative temperature change ($\Delta T < 0$) and lower α_c/α_s is used for the applications with positive temperature change ($\Delta T > 0$).

VALIDATION OF MODEL

Another goal of this work is to make a quantitative comparison between the experiments and the theoretical model of the previous sections. It was emphasized in the Experimental Procedures and Results and Discussion sections that the residual stress change in the coating under the temperature variation has a profound influence on the corrosion rate at the coating/substrate interface. Corrosion rate in mm/y is calculated by using:⁷⁵

$$\text{Corrosion rate} = 3.27 \times 10^{-3} \left(\frac{i \times EW}{\rho} \right) \quad (35)$$

where i is the corrosion current density calculated from Equation (25), ρ is the density of steel in g/cm^3 , and EW is the equivalent weight in grams of steel. Figure 13 shows the experimental result plotted using the mean of data values from three corrosion sensors for the initial two 20 h steps. Figure 13 also shows a typical simulation result at specific conditions for which an experiment has been performed. A comparative analysis between experimental and simulation results showed that for the first step when ΔT is equal to 0 ± 1 K, the corrosion rate is negligible for both experimental and simulation results. For the second step during 10 h to 14 h, indicated as point A when ΔT starts to decrease, the simulation result showed a slight increase in the corrosion rate. However, during the experiment for this short interval of time (10 h to 14 h), no change in the corrosion rate was observed. This perhaps can be attributed to the low sensitivity of corrosion sensors to the incipient electrochemical activity. For the next 14 h to 17 h, indicated as point B when the temperature reaches its lowest point for the whole experiment, the simulation result showed a sudden rise-fall trend maintaining the maximum corrosion rate during this time. A similar behavior with high

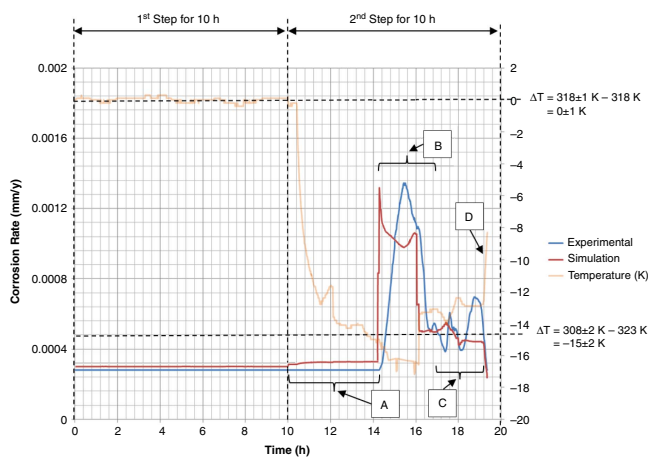


FIGURE 13. Comparative analysis between experimental and simulation results to validate the model.

corrosion rate was also observed for the experimental result, but the rise-fall behavior was not as sharp as for the simulation result. From 17 h to 19 h, represented as point C, the trends for both the simulation and experimental results showed similar behavior in a way that the corrosion rate was high for low-temperature peaks and low for high-temperature peaks. And finally after 19 h at point D, the corrosion rate started to decrease with increasing temperature. The comparison between experimental data and simulation results in Figure 13 shows a satisfactory agreement. In the simulation, the model overpredicts the corrosion rate for short-term experiments (20 h), which makes some of the data points in the simulation graph deviate from the experimental data points.

CONCLUSIONS

- ❖ The performance of coating-substrate system has been investigated in the presence of residual stress under the frame work of material science, solid mechanics, and electrochemistry. Based on novel self-consistent equations for corrosion current density, the effects of temperature, moduli ratio, thickness ratio, thermal mismatch ratio, and residual stress gradient of coating and substrate are addressed with the help of the Newton Rhapsom method. The results show that for the case when coefficient of thermal expansion (CTE) of the coating is greater than substrate, the negative change in temperature ($\Delta T < 0$ K) accounts for the same direction of residual stress as of the diffusion stress. This behavior increases the deflection of coating-substrate system and results in tensile residual stress in the coating. The tensile behavior opens the pre-existing microcracks in the coating and, therefore, allows the diffusion of corrosive agents before reaching the saturation state of corrosive agents in coating. The increase in the diffusion rate also increases the corrosion current density at the interface of coating and substrate. After reaching the saturation state at a certain time, the corrosion current density becomes constant; therefore, residual stress plays a critical role in the corrosion current density only before the time period when the saturation condition is reached. However, the effect of residual stress on the corrosion current density gradually disappears after the saturation condition of corrosive agents is reached.
- ❖ The results also show that a larger modulus ratio E_c/E_s accounts for higher corrosion current density; therefore, to achieve the better performance of coating-substrate system, it is always better to use a smaller modulus ratio. For the case when $\Delta T < 0$ K, the corrosion current density decreases first, and then becomes stable with increasing ratio of thickness s/h . However, for the case when $\Delta T > 0$ K,

the corrosion current density is constant for all thickness ratios s/h . Therefore, increasing the thickness of coating is not necessarily better for achieving higher performance of coating-substrate system in terms of corrosion. For the condition where $\Delta T < 0$ K, the corrosion current density increases with the decrease in the CTE mismatch between coating and substrate. However, for the condition where $\Delta T > 0$ K, the corrosion current density decreases with the decrease in the CTE mismatch. Therefore, for higher performance in terms of corrosion, it is better to use higher α_c/α_s for the applications with negative temperature change ($\Delta T < 0$) and lower α_c/α_s for the applications with positive temperature change ($\Delta T > 0$).

❖ A model experiment was performed in conjunction with the analysis. The experiment showed good, quantitative agreement with the trends predicted by the theory. Furthermore, the experiment emphasized the important role that the residual stress resulting from temperature change plays in the evolution of corrosion current density at the coating/substrate interface.

ACKNOWLEDGMENTS

This research is joint funded by Defence Science and Technology Laboratory (DSTL), Ministry of Defence (MoD), and Bournemouth University U.K. The authors acknowledge their support and contributions.

REFERENCES

1. A. Stierle, *Science* 321, 5887 (2008): p. 349-350.
2. D.A. Jones, *Principles and Prevention of Corrosion* (New York, NY: Pearson Education, 2014).
3. B. Wessling, J. Posdorfer, *Electrochim. Acta* 44, 12 (1999): p. 2139-2147.
4. F.L. LaQue, *Marine Corrosion: Causes and Prevention* (New York, NY: Wiley-Blackwell, 1975).
5. C.G. Munger, L.D. Vincent, *Corrosion Prevention by Protective Coatings* (Houston, TX: NACE International, 1999).
6. W.-K. Lu, R.L. Elsenbaumer, B. Wessling, *Synthetic Metals* 71, 1 (1995): p. 2163-2166.
7. X. Zhao, P. Munroe, D. Habibi, Z. Xie, *J. Asian Ceramic Societies* 1, 1 (2013): p. 86-94.
8. D.P. Riemer, M.E. Orazem, "Modeling Coating Flaws with Non-Linear Polarization Curves for Long Pipelines," in *Corrosion and Cathodic Protection Modeling and Simulation*, ed. R.A. Adey, Advances in Boundary Elements, vol. 12 (Southampton, United Kingdom: WIT Press, 2006): p. 225-259.
9. K. Holmberg, A. Mathews, *Thin Solid Films* 253, 1 (1994): p. 173-178.
10. M. Kaufman, J. Fink, *Acta Metall.* 36, 8 (1988): p. 2213-2228.
11. T. Magnin, R. Chieragatti, R. Oltra, *Acta Metall. Mater.* 38, 7 (1990): p. 1313-1319.
12. K. Sieradzki, R. Newman, *J. Phys. Chem. Solids* 48, 11 (1987): p. 1101-1113.
13. W.-Y. Chu, J. Yao, C.-M. Hsiao, *Corrosion* 40, 6 (1984): p. 302-306.
14. X. Liu, G. Frankel, *Corros. Sci.* 48, 10 (2006): p. 3309-3329.
15. D.S. Campbell, "Mechanical Properties of Thin Films," in *Handbook of Thin Film Technology*, eds. L.I. Maissel, R. Glang, chpt. 12 (New York, NY: McGraw-Hill, 1970).
16. X. Feng, Y. Huang, A. Rosakis, *J. Appl. Mech.* 74, 6 (2007): p. 1276-1281.
17. S. Huang, X. Zhang, *Sensors and Actuators A* 134, 1 (2007): p. 177-185.
18. H. Soliman, A. Waheed, *J. Mater. Sci. Technol.* 15, 5 (1999): p. 457-462.
19. T. Clyne, S. Gill, *J. Thermal Spray Technol.* 5, 4 (1996): p. 401-418.
20. S. Widjaja, A.M. Limarga, T.H. Yip, *Thin Solid Films* 434, 1 (2003): p. 216-227.
21. X. Zhang, B. Xu, H. Wang, Y. Wu, *Thin Solid Films* 488, 1 (2005): p. 274-282.
22. M. Wisnom, M. Gigliotti, N. Ersoy, M. Campbell, K. Potter, *Composites Part A: Appl. Sci. Manufacturing* 37, 4 (2006): p. 522-529.
23. P. Bansal, P. Shipway, S. Leen, *Acta Mater.* 55, 15 (2007): p. 5089-5101.
24. M.S. Ahmed, P. Munroe, Z.-T. Jiang, X. Zhao, W. Rickard, Z.-F. Zhou, L.K.Y. Li, Z. Xie, *Corros. Sci.* 53, 11 (2011): p. 3678-3687.
25. E. Busso, J. Lin, S. Sakurai, M. Nakayama, *Acta Mater.* 49, 9 (2001): p. 1515-1528.
26. I. Spitsberg, D. Mumm, A. Evans, *Mater. Sci. Eng. A* 394, 1 (2005): p. 176-191.
27. Y.S. Podstrigach, P. Shevchuk, *Soviet Materials Science: a translation of Fiziko-Khimicheskaya Mekhanika Materialov/ Academy of Sciences of the Ukrainian SSR* 3, 5 (1968): p. 420-426.
28. Y. Ida, *J. Geophysical Research* 74, 12 (1969): p. 3208-3218.
29. F. Larché, J. Cahn, *Acta Metall.* 21, 8 (1973): p. 1051-1063.
30. W.B. Kamb, *J. Geophysical Research* 66, 1 (1961): p. 259-271.
31. F. Larché, J. Cahn, *Acta Metall.* 30, 10 (1982): p. 1835-1845.
32. G.B. Stephenson, *Acta Metall.* 36, 10 (1988): p. 2663-2683.
33. T. Nguyen, J. Hubbard, J. Pommersheim, *J. Coatings Technol.* 68, 855 (1996): p. 45-56.
34. Y. Prawoto, N. Kamsah, M.M. Yajid, Z. Ahmad, *Theoretical Appl. Fracture Mech.* 56, 2 (2011): p. 89-94.
35. F. Yang, J. Li, *J. Appl. Phys.* 93, 11 (2003): p. 9304-9309.
36. A.I. Rusanov, *Surf. Sci. Reports* 58, 5 (2005): p. 111-239.
37. A. Saeed, Z. Khan, M. Clark, M. Nel, R. Smith, *Insight-Non-Destructive Testing and Condition Monitoring* 53, 7 (2011): p. 382-386.
38. A. Saeed, Z.A. Khan, M. Hadfield, S. Davies, *Tribology Trans.* 56, 4 (2013): p. 637-644.
39. A. Saeed, Z.A. Khan, E. Montgomery, *Mater. Perform. Characterization* 2, 1 (2013): p. 1-16.
40. Z.A. Khan, P. Pashaei, R.S. Bajwa, M.H. Nazir, M. Camak, *Int. J. Computational Methods & Experimental Measurements* 3, 2 (2015): p. 165-174.
41. M.H. Nazir, Z. Khan, K. Stokes, *J. Adhesion Sci. Technol.* 29, 5 (2014): p. 392-423.
42. M.H. Nazir, Z.A. Khan, K. Stokes, *J. Adhesion Sci. Technol.* 29, 14 (2015): p. 1415-1445.
43. M.H. Nazir, Z.A. Khan, K. Stokes, *J. Adhesion Sci. Technol.* 29, 22 (2015): p. 2475-2513.
44. M.H. Nazir, Z.A. Khan, K. Stokes, *J. Adhesion Sci. Technol.* 29, 12 (2015): p. 1200-1228.
45. M.H. Nazir, Z.A. Khan, *Int. J. Computational Methods & Experimental Measurements* 3, 4 (2015): p. 316-328.
46. Z.A. Khan, M. Grover, M.H. Nazir, "The Implications of Wet and Dry Turning on the Surface Quality of EN8 Steel," in *Transactions on Engineering Technologies*, eds. G.-C. Yang, S.-L. Ao, L. Gelman (New York, NY: Springer, 2015), p. 413-423.
47. M.H. Nazir, Z.A. Khan, A. Saeed, K. Stokes, *Eng. Failure Anal.* 63 (2016): p. 43-60.
48. A. Saeed, Z.A. Khan, M.H. Nazir, *Sustainability* 7, 12 (2015): p. 16451-16464.
49. M.H. Nazir, Z.A. Khan, A. Saeed, K. Stokes, "A Model for Cathodic Blister Growth in Coating Degradation Using Mesomechanics Approach," *Werkst. Korros.* in press (2016): doi: <http://dx.doi.org/10.1002/maco.201508562>.
50. D.R. Lide, *CRC Handbook of Chemistry and Physics* (Boca Raton, FL: CRC Press, 2004).
51. D.W. Brown, R.J. Connolly, D.R. Darr, B. Laskowski, "Linear Polarization Resistance Sensor Using the Structure as a Working Electrode," *European Conference of the Prognostics and Health Management Society* (Rochester, NY: PHM Society, 2014): p. 1-7.
52. D. Brown, D. Darr, J. Morse, B. Laskowski, "Theoretical and Experimental Evaluation of a Real-Time Corrosion Monitoring

- System for Measuring Pitting in Aircraft Structures," *First European Conference of the Prognostics and Health Management Society* (Rochester, NY: PHM Society, 2012): p. 1-9.
53. V. Feliu, J. González, C. Andrade, S. Feliu, *Corros. Sci.* 40, 6 (1998): p. 995-1006.
54. ASTM E831-1451, "Standard Test Method for Linear Thermal Expansion of Solid Materials by Thermomechanical Analysis" (West Conshohocken, PA: ASTM, 2014).
55. ASTM E2769-13, "Standard Test Method for Elastic Modulus by Thermomechanical Analysis Using Three-Point Bending and Controlled Rate of Loading" (West Conshohocken, PA: ASTM, 2013).
56. W. Wilson, I.-W. Yu, *Int. J. Fracture* 15, 4 (1979): p. 377-387.
57. Z. Tang, F. Wang, W. Wu, *Oxidation of Met.* 48, 5-6 (1997): p. 511-525.
58. C.-H. Hsueh, *J. Appl. Phys.* 91, 12 (2002): p. 9652-9656.
59. M. Stratmann, A. Leng, W. Fürbeth, H. Streckel, H. Gehmecker, K.-H. Große-Brinkhaus, *Progress in Organic Coatings* 27, 1 (1996): p. 261-267.
60. A. Leng, H. Streckel, M. Stratmann, *Corros. Sci.* 41, 3 (1998): p. 579-597.
61. M. Stratmann, R. Feser, A. Leng, *Electrochim. Acta* 39, 8 (1994): p. 1207-1214.
62. K.J. Laidler, *J. Chemical Education* 61, 6 (1984): p. 494.
63. M.-W. Huang, C. Allely, K. Ogle, M.E. Orazem, *J. Electrochem. Soc.* 155, 5 (2008): p. C279-C292.
64. O.D. Kellogg, *Foundations of Potential Theory* (New York, NY: Springer, 1929).
65. L. Mejlbro, "The Complete Solution of Fick's Second Law of Diffusion with Time-Dependent Diffusion Coefficient and Surface Concentration," *Proc. of the Durability of Concrete in Saline Environment*, ed. P. Sandberg (Lund, Sweden: Cementa AB, 1996), p. 127-158.
66. G. Cowper, *J. Appl. Mech.* 33, 2 (1966): p. 335-340.
67. F.-Z. Xuan, L.-Q. Cao, Z. Wang, S.-T. Tu, *Computational Mater. Sci.* 49, 1 (2010): p. 104-111.
68. W. David, M. Thackeray, L. De Picciotto, J. Goodenough, *J. Solid State Chem.* 67, 2 (1987): p. 316-323.
69. S. Prussin, *J. Appl. Phys.* 32, 10 (1961): p. 1876-1881.
70. X. Zhang, W. Shyy, A.M. Sastry, *J. Electrochem. Soc.* 154, 10 (2007): p. A910-A916.
71. K.N. Allahar, M.E. Orazem, K. Ogle, *Corros. Sci.* 49, 9 (2007): p. 3638-3658.
72. K.N. Allahar, "Mathematical Modeling of Disbonded Coating and Cathodic Delamination Systems" (Ph.D. diss., University of Florida, 2003).
73. J. Newman, *Electrochemical Engineering* (Englewood Cliffs, NJ: Prentice-Hall, 1991).
74. D. Sheen, *Introduction to Numerical Analysis* (New York, NY: Springer, 1980).
75. ASTM G59-97, "Standard Test Method for Conducting Potentiodynamic Polarization Resistance Measurements" (West Conshohocken, PA: ASTM International, 2009).

NOMENCLATURE

Unless otherwise specified, the following nomenclature is used in this paper.

Notation Description

ΔT	Temperature difference/change
α_c and α_s	Coefficient of thermal expansion (CTE) of coating and substrate, respectively
E_c and E_s	Young's modulus of coating and substrate, respectively
h	Thickness of coating
s	Thickness of substrate
σ_r	Residual stress
R_p	Polarization resistance

B	Stern-Geary constant
$i = B/R_p$	Corrosion current density
c_{k_B}	Bulk ionic concentration
Φ	Solution potential
Z_k	Charge number of corrosive species
x	Distance to the defect
t_D	Diffusion time
$D_{S,STA_{ion}}$	Diffusion coefficient of the corrosive species along the interface
RH	Pore relative humidity
t_{exp}	Time of exposure
D_k	Average of standard diffusion coefficient of all of the corrosive species
RH_{STA}	Standard relative humidity
T_{STA}	Standard temperature
t_{STA}	Time of exposure at which D_k is measured (normally 1 month)
G_a	Activation energy of corrosive species
R	Universal gas constant
t_a	Actual time of exposure
n_{ag}	Age reduction factor
$c_{k_{RH}}$	Threshold concentration of species
η	The mobility constant of cations
t	Time passed after the defect confronts the solution
t_n	The time required to activate the defect
c_{k_o}	The equilibrium concentration of ions at the interface in contact with the bulk solution c_{k_B}
$K_{Ck_{eq}} = c_{k_o}/c_{k_B}$	Equilibrium constant
μ_k^o	Chemical potential in the given standard state
σ_m	Stress tensor
$\sigma_i = \sigma_{d_i} + \sigma_{r_i}$	Principle stresses (sum of residual stress and diffusion induces stress)
\bar{V}_{P_k}	Partial molar volume of diffusing species k
V_{m_k}	Molar volume of solution
P	Pressure
n_k	Molar concentration of diffusing species
J_k	Diffusion flux of species k
\mathcal{E}	Strain distribution
\mathcal{E}_{u_r}	Uniform component of residual strain
\mathcal{E}_b	Bending component of strain
ζ_r	Radius of curvature resulting from residual stress
\mathcal{E}_{u_d}	Uniform component of diffusion-induced strain
ζ_d	Radius of curvature resulting from diffusion-induced stress
$E_{O_2}^o$	Equilibrium potential of oxygen
E	Substrate potential
β_{O_2}	Oxygen Tafel slope
$\frac{1}{s_{d,d}}$ and $\frac{1}{s_{d,nd}}$	Bending curvatures resulting from diffusion-induced stress for delaminated and nondelaminated coating, respectively

$\frac{1}{\epsilon_{rd}}$ and $\frac{1}{\epsilon_{rnd}}$	Bending curvatures resulting from residual stress for delaminated and nondelaminated coating, respectively	$i_{O_2}^{coat}$	Current density resulting from the oxygen reduction at any position along the coating/substrate interface
c_{O_2}	Dissolved concentration of oxygen at coating surface	i^s	Current density resulting from substrate dissolution
D_{O_2}	Diffusion coefficients for oxygen	$i = i_{O_2}^{coat} + i^s$	Corrosion current density along the interface of coating and substrate
n	The number of electrons transferred		